

Emergent ac Effect in Nonreciprocal Coupled Condensates

Ji Zou,¹ Valerii K. Kozin,¹ Daniel Loss,¹ and Jelena Klinovaja¹

¹*Department of Physics, University of Basel, Klingelbergstrasse 82, 4056 Basel, Switzerland*

(Dated: December 30, 2025)

We report an emergent ac Josephson-like effect arising without external bias, driven by the interplay between nonreciprocity and nonlinearity in coupled condensates. Using a minimal model of three mutually nonreciprocally coupled condensates, we uncover a rich landscape of dynamical phases governed by generalized Josephson equations. This goes beyond the Kuramoto framework owing to inherent nonreciprocity and dynamically evolving effective couplings, leading to static and dynamical ferromagnetic and (anti)vortex states with nontrivial phase winding. Most strikingly, we identify an ac phase characterized by the emergence of two distinct frequencies, which spontaneously break the time-translation symmetry: one associated with the precession of the global $U(1)$ Goldstone mode and the other with a stabilized limit cycle in a five-dimensional phase space. This phase features bias-free autonomous oscillatory currents beyond conventional Josephson dynamics. We further examine how instabilities develop in the ferromagnetic and vortex states, and how they drive transitions into the ac regime. Interestingly, the transition is hysteretic: phases with different winding numbers destabilize under distinct conditions, reflecting their inherently different nonlinear structures. Our work lays the foundation for exploring nonreciprocity-driven novel dynamical phases in a broad class of condensate platforms.

Interacting condensates exhibit rich dynamical phenomena. A hallmark example is the Josephson effect [1], where a static phase difference induces a dc current without external bias, while a frequency mismatch, typically driven by a bias, leads to an ac current. These phenomena have far-reaching impact across physics, from condensed matter and atomic systems to quantum information science. The study of coupled condensate dynamics now spans a diverse array of platforms, including ultracold atomic gases [2], exciton–polariton condensates [3], photonic systems [4], and magnon condensates [5–7].

In realistic settings, condensates inevitably interact with their environment, leading to decay. While dissipation is traditionally regarded as detrimental [8–10], recent studies have revealed that dissipative couplings (or collective decay), either intrinsic or engineered, can enable nonreciprocal interactions. Such nonreciprocity has emerged as a powerful resource for controlling transport and nonequilibrium phenomena, giving rise to diode-like behavior [11, 12], unidirectional amplification [13], enhanced quantum entanglement [14–17], and nonreciprocal phase transitions [18]. Yet, the role of nonreciprocity in the dynamics of coupled condensate systems remains largely unexplored. This raises an interesting question: What new phenomena emerge when nonreciprocal interactions are introduced into phase-coherent interacting condensates with intrinsic nonlinearity?

Here, we show that nonreciprocity, together with nonlinearity, gives rise to a novel dynamical phase, featuring the spontaneous emergence of two distinct frequencies and self-sustained oscillatory currents in the absence of any external bias, going beyond the conventional ac Josephson effect and reminiscent of time-crystalline behavior [20–23]. We demonstrate this phenomenon by considering a minimal model of three nonreciprocally cou-

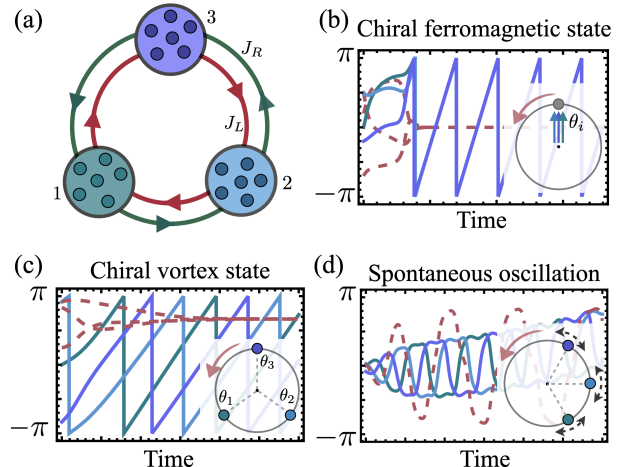


FIG. 1. (a) Schematic of three mutually nonreciprocally coupled condensates, with asymmetric couplings J_L and J_R . (b) Chiral ferromagnetic phase, where all condensates share the same phase and undergo collective precession at a constant frequency. (c) Chiral vortex phase, characterized by a phase winding of 2π across the three sites; relative phases are locked while the global phase rotates uniformly. (d) Spontaneous ac phase, featuring two emergent frequencies: one associated with global phase rotation and the other with oscillations of the relative phases. Dashed red: relative phase evolution θ_{ij} ; solid lines: individual phases $\theta_i(t)$ [19].

pled condensates, as illustrated in Fig. 1(a). By deriving the generalized Josephson equations for the system, we reveal how the interplay between nonreciprocal interactions and intrinsic nonlinearity give rise to a rich landscape of dynamical phases. We find both static and dynamical (chiral) ferromagnetic states, where all phases are locked [see Fig. 1(b)], as well as (anti)vortex states characterized by nonzero phase winding, as shown in

Fig. 1(c). We further investigate how instabilities develop within these phases and trigger transitions into the ac regime [see Fig. 1(d)]. Interestingly, we find that the instability is path-dependent: distinct winding numbers destabilize under different conditions, revealing how topology shapes the nonlinear structure. We understand the emergence and transition between these phases using insights from bifurcation theory.

Model and generalized Josephson equations—We consider a model of three coupled condensates, each described by a macroscopic wavefunction $\psi_i = \sqrt{N_i}e^{i\theta_i}$ for $i \in \{1, 2, 3\}$, where N_i and θ_i denote the particle number and phase, respectively. The system evolves according to [24] $i\hbar\partial_t\psi_i = (\Delta_i - i\gamma)\psi_i + J_L\psi_{i+1} + J_R\psi_{i-1}$. We will assume no external bias, i.e., $\Delta_i = \Delta_0$ for all i , and set $\Delta_0 = 0$ by moving to the rotating frame. The first term accounts for local losses in each condensate with rate $\gamma > 0$, while the last two terms capture nonreciprocal coupling between them, with $J_L = \mathcal{J} - iG/2 = J + i(D - G/2)$ and $J_R = \mathcal{J}^* - iG/2 = J - i(D + G/2)$. Here, $\mathcal{J} = J + iD$ denotes the coherent coupling consisting of symmetric J and antisymmetric D components. An important ingredient in this study is the parameter G , which quantifies the strength of the dissipative coupling. Stability of the system requires $|G| \leq \gamma$ (to avoid net gain). In different physical platforms, such coupling can arise through various mechanisms. For instance, in magnon condensates, the dissipative coupling naturally emerges via nonlocal spin transfer across non-magnetic spacers [25–27]; in photonic systems, it can be engineered through tailored reservoirs or auxiliary lossy modes [13, 28–30]; and in ultracold atom setups, nonreciprocal coupling can be implemented using chiral waveguides or structured optical reservoirs [31–33].

We now derive the generalized Josephson equations for the system. For notational clarity, we define the unit vector $\vec{n}(\theta_{ij}) \equiv (\cos\theta_{ij}, \sin\theta_{ij})$ associated with the relative angle of the condensates $\theta_{ij} = \theta_i - \theta_j$, and introduce time-dependent effective coupling vectors:

$$\vec{J}_i^L(t) = \sqrt{N_{i+1}/N_i}(\text{Re } J_L, \text{Im } J_L), \quad (1)$$

$$\vec{J}_i^R(t) = \sqrt{N_{i-1}/N_i}(\text{Re } J_R, \text{Im } J_R), \quad (2)$$

which describe clockwise and counterclockwise particle tunneling, respectively. The generalized Josephson equations then take the compact form:

$$d\theta_i/dt = -\vec{J}_i^L(t) \cdot \vec{n}(\theta_{i,i+1}) - \vec{J}_i^R(t) \cdot \vec{n}(\theta_{i,i-1}). \quad (3)$$

Importantly, the couplings $\vec{J}_i^{L/R}(t)$ depend dynamically on the particle numbers $N_i(t)$, which evolve as:

$$dN_i/dt = -2N_i\hat{z} \cdot [\vec{J}_i^L(t) \times \vec{n}(\theta_{i,i+1}) + \vec{J}_i^R(t) \times \vec{n}(\theta_{i,i-1})] - 2\gamma N_i + \mathcal{P}, \quad (4)$$

where \mathcal{P} denotes a constant pump just used to sustain finite condensates. We choose $\mathcal{P} = \gamma$ without loss of

generality. These equations exhibit strong nonlinearity with dynamical feedback between particle numbers and phases. We note that the system is invariant under a global phase shift $\theta_i \rightarrow \theta_i + \varphi$, reflecting a continuous U(1) symmetry with no preferred phase. As we will show, this symmetry can be spontaneously broken in static phases and dynamically restored in chiral phases. Moreover, the absence of explicit driving guarantees time-translation invariance, which can likewise be broken.

We stress that Eq. (3) goes beyond the Kuramoto model of synchronization with two important features: the dynamical nature of the coupling strengths and the intrinsic nonreciprocity of the interactions. The full phase space of this coupled condensate system is six-dimensional, forming a manifold $\mathbf{V} = (\theta_i, N_i) \in \mathbb{T}^3 \times \mathbb{R}_+^3$. The dynamics on this manifold are inherently nonlinear and nonreciprocal, leading to quite intricate nonequilibrium behavior.

As a starting point and also to build physical intuition, we begin by considering the steady state case where the particle numbers are constant and $N_i = N_0 = \text{constant}$ due to the rotation symmetry [Fig. 1(a)]. In this case, the model [Eqs. (3) and (4)] reduces to the nonreciprocal Kuramoto model [18]. To gain insight, we examine the interaction on a single link. We write the evolution equations as

$$d\theta_1/dt = -J \cos\theta_{21} + (D - G/2) \sin\theta_{21}, \quad (5)$$

$$d\theta_2/dt = -J \cos\theta_{21} + (D + G/2) \sin\theta_{21}. \quad (6)$$

We observe that the coherent couplings J and D contribute equally to the evolution of the phases, modifying the overall rotation rate. In contrast, the dissipative coupling G directly governs the evolution of the relative phase via $d\theta_{21}/dt = G \sin\theta_{21}$. When $G < 0$, this term favors alignment of neighboring phases, effectively acting as a ferromagnetic interaction that leads the three condensates to synchronize into a uniform phase-locked state. In sharp contrast, for $G > 0$, the dissipative coupling favors anti-alignment between neighboring phases. This would introduce frustration in the three coupled condensates. In this regime, such dissipation-induced frustration leads to non-collinear configurations, resulting in a vortex or antivortex state characterized by relative phases of $\pm 2\pi/3$ across the three sites, yielding a total winding of $\pm 2\pi$. Thus, in the nonreciprocal Kuramoto model [34], the final state is either a ferromagnetic configuration [Fig. 1(b)] or an (anti)vortex state [Fig. 1(c)], dictated solely by the sign of the dissipative coupling G . A detailed analysis, along with numerical results, is provided in SM [34] for the nonreciprocal Kuramoto model. We next examine the stability and evolution of these phases in the full dynamics governed by Eqs. (3) and (4).

Ferromagnetic phase and its instability—Here, we focus on the ferromagnetic state and investigate how in-

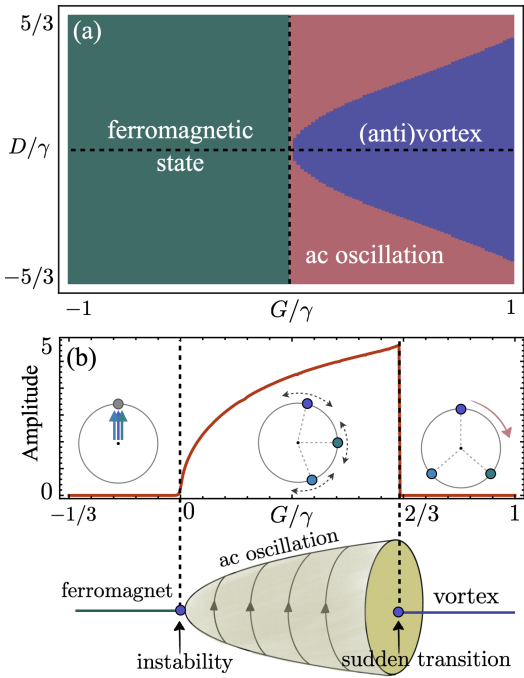


FIG. 2. (a) Phase diagram showing the ferromagnetic state and its transition to other phases upon instability for $J = 0$. It is obtained by numerically solving the generalized Josephson equations starting from initial conditions near the ferromagnetic fixed point [35]. (b) Steady-state oscillation amplitude of θ_{21} as a function of dissipative coupling G for $D/\gamma = 1$ and $J = 0$ obtained [35].

stabilities arise, driving transitions to other dynamical regimes. Although the nonequilibrium nature of the system precludes a free energy description, distinct phases and their transitions can be identified by analyzing the generalized Josephson equations (3) and (4). While the full dynamics remain analytically intractable, we assess the stability of the ferromagnetic state by introducing small perturbations $\delta\mathbf{V}$ around the ferromagnetic steady state \mathbf{V}_F , leading to $\partial_t\delta\mathbf{V} = \hat{\mathcal{L}}_F\delta\mathbf{V}$. Here, $\hat{\mathcal{L}}_F$ is a linear operator acting on the tangent space of the phase-space manifold at \mathbf{V}_F . A key feature of this operator is that it always possesses a zero eigenvalue, corresponding to the Goldstone mode associated with the broken $U(1)$ symmetry, namely the global phase $\Phi = \sum_i \theta_i/3$ [36].

To isolate the nontrivial dynamics, we exploit this symmetry and decompose the phase degrees of freedom into the zero mode Φ and two independent relative phases, θ_{21} and θ_{32} . This allows us to reduce the dynamics to a five-dimensional effective phase space $\mathcal{V} = (\theta_{21}, \theta_{32}, N_i) \in \mathbb{T}^2 \times \mathbb{R}_+^3$, which we denote as \mathcal{M} . The stability of the ferromagnetic phase is governed by the reduced linear operator (see SM [34]), which has the structure:

$$\hat{\mathcal{L}}_F = \begin{pmatrix} \mathcal{L}_F^\theta & J\mathcal{L}_1 \\ J\mathcal{L}_2 & \mathcal{L}_F^N \end{pmatrix}. \quad (7)$$

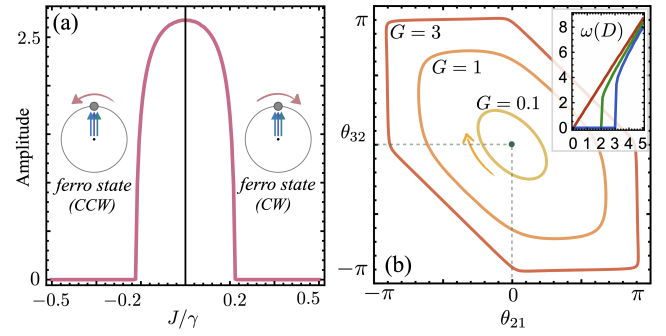


FIG. 3. (a) Steady-state oscillation amplitude of θ_{21} as a function of coupling J for $D/\gamma = 1.2$ and $G/\gamma = 0.1$. (b) Projected trajectories of persistent oscillations on the reduced phase space \mathcal{M} at $J = 0$, shown on the \mathbb{T}^2 submanifold of relative phases, for varying values of G (with $\gamma = 3$, $D = 5$). Inset: oscillation frequency as a function of D , for $G = 0$ (red), $G = 1$ (green), and $G = 3$ (blue), with $\gamma = 3$ fixed. Both plots are produced from long-time numerical solutions of the generalized Josephson equation, starting near the ferromagnetic fixed point [35].

It acts on \mathcal{M} around the ferromagnetic fixed point $\mathbf{V}_F = (0, 0, N_i = N_0)$, with $N_0 = \gamma/[2(\gamma + G)]$. Here, \mathcal{L}_F^θ and \mathcal{L}_F^N act on \mathbb{T}^2 and \mathbb{R}_+^3 respectively, while \mathcal{L}_1 and \mathcal{L}_2 encode coupling between them. The ferromagnetic phase remains stable when $\hat{\mathcal{L}}_F$ is Hurwitz (all eigenvalues have negative real parts), ensuring that perturbations are damped over time. Instability emerges when any eigenvalue crosses into the right half-plane, marking a dynamical phase transition. We show that the ferromagnetic phase is stable when [34]

$$G(G + 4\gamma) < 12J^2. \quad (8)$$

Unlike the nonreciprocal Kuramoto model [34], where the ferromagnetic phase is stable only for $G < 0$, we find that coherent coupling J extends its stability into the $G > 0$ regime. This arises from the structure of $\hat{\mathcal{L}}_F$ and reflects the nontrivial interplay between phase and number dynamics: the number sector, governed by \mathcal{L}_F^N , is intrinsically stable [34], and its coupling through J to the phase sector suppresses emerging instabilities. In this way, number dynamics acts as a dynamical stabilizer, reinforcing the robustness of the ferromagnetic phase beyond its decoupled limit.

We show the phase diagram in Fig. 2(a) for $J = 0$ (see SM for more cases [34]). Interestingly, the ferromagnetic phase does not immediately transition into a (anti)vortex state. Instead, it first enters a dynamical regime characterized by persistent oscillations on the reduced phase space \mathcal{M} , with no equilibrium analogue. When the dissipative coupling G exceeds a critical threshold, the system eventually settles into an (anti)vortex state. Figure 2(b) shows the steady-state oscillation amplitude of θ_{21} for fixed D . For $G < 0$, the system resides in a ferromagnetic state that breaks the global $U(1)$ symmetry. This

state is generically dynamical for finite J : the Goldstone mode Φ exhibits uniform rotation at frequency $\Omega = -2J$, dynamically restoring $U(1)$ symmetry on average, a hallmark of the chiral phase in nonreciprocal systems [18]. However, unlike previous works that rely on stochastic noise to stabilize chiral phases [18], the interacting condensate system realizes them purely through its internal dynamical structure, without invoking any other ingredients. We show such chiral ferromagnetic rotation in Fig. 3(a) and also include an example of the emergence of this chiral ferromagnetic phase in the condensate dynamics in Supplemental Video 1 [34], starting from an initial state near the ferromagnetic fixed point.

As G becomes positive, the system enters a richer dynamical regime: beyond global phase rotation (with frequency proportional to J), the system develops autonomous oscillations on \mathcal{M} at a distinct frequency. To visualize this, we project the oscillatory trajectory onto the \mathbb{T}^2 submanifold in Fig. 3(b). These persistent relative-phase oscillations generate oscillatory particle currents between condensates, accompanied by corresponding modulations in particle numbers. Interestingly, this ac-Josephson-like effect emerges intrinsically from the nonreciprocity and nonlinearity of the system. It is principally distinct from conventional ac effects driven by external bias, which is set to zero in this study. We show this ac phase in the condensate dynamics, with two emergent frequencies, in Supplemental Video 2 [34]. From the perspective of dynamical systems, the transition from the ferromagnetic state to persistent ac oscillations is a manifestation of a Poincaré–Andronov–Hopf bifurcation [37] occurring on the five-dimensional manifold \mathcal{M} , which originates from a mechanism distinct from that of the chiral phase. At the Hopf threshold $G_c = 2[(3J^2 + \gamma^2)^{1/2} - \gamma]$, oscillations of relative angles emerge with amplitude A scaling as $A^2 \propto G/2 - \gamma + \sqrt{(G + \gamma)^2 - 9J^2}$. In Fig. 3(b), we observe a clear increase in oscillation amplitude with increasing G ; its dependence on J is also displayed in Fig. 3(a). Meanwhile, the oscillation frequency is shown to be $\omega = \sqrt{3}D + \mathcal{O}(G - G_c)$ [see inset of Fig. 3(b)]. The ac phase therefore exhibits spontaneous breaking of time-translation symmetry through the emergence of two independent frequencies, reminiscent of time-crystalline behavior [20]: one originates from the coherent rotation of the $U(1)$ zero mode (with frequency Ω) and the other from stable limit cycles on \mathcal{M} (with frequency ω).

The ac oscillation phase remains stable until the limit-cycle amplitude exceeds a critical threshold, as shown in Fig. 2(b). Beyond this point, the trajectory on \mathcal{M} escapes the oscillatory attractor and transitions into a topologically distinct fixed point corresponding to the (anti)vortex phase (see Supplemental Video 3 [34]). This sudden change is a manifestation of a global bifurcation [37], fundamentally different from the Hopf-type

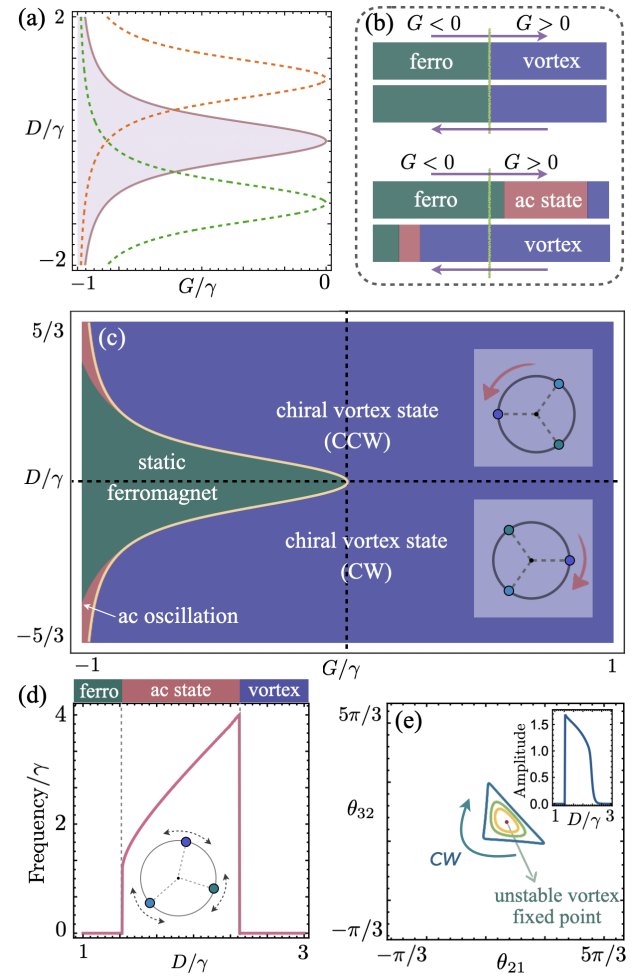


FIG. 4. (a) Instability boundary of the vortex phase for different J . Red: $J = 0$; orange: $J/\gamma = -\sqrt{3}$; green: $J/\gamma = \sqrt{3}$. The shaded region marks the parameter space where the vortex state is unstable for $J = 0$. (b) Upper panel: In the nonreciprocal Kuramuro model [34], both the ferromagnetic state (green) and the vortex state (purple) lose stability exactly at $G = 0$, switching directly into each other. Lower panel: For the full dynamics, the ferromagnetic phase (green) first destabilises at a positive G , entering an intermediate ac state (red) before reaching the vortex phase (purple); conversely, the vortex phase becomes unstable at a negative G . The separation of these thresholds evidences hysteresis. (c) Phase diagram showing the vortex phase and its transition to other phases for $J = 0$, which is obtained numerically. The yellow curve shows the analytically obtained instability boundary given by Eq. (9), which agrees well with the numerics. (d) Frequency ω of the steady state as a function of D for $J = 0$ and $G/\gamma = -0.98$. (e) Limit-cycle trajectories projected onto the relative-phase torus \mathbb{T}^2 for $J = 0$ and $G/\gamma = -0.98$. From inner to outer trajectories, we set $D/\gamma = 2.7, 2.6, 1.5$. Inset: oscillation amplitude versus D . Plots (c)–(e) are obtained from numerical solutions of the generalized Josephson equations, starting near the vortex fixed point [38].

transition [see Fig. 2(b)] that initiates the ac phase.

Instability of vortex state—Having reached the vortex phase, we now turn to its stability. Interestingly, starting from the vortex state reveals a distinct phase diagram and instability condition compared to Fig. 2(a). To analyze this, we introduce small perturbations around the vortex fixed point, $\mathbf{V}_V = (2\pi/3, 2\pi/3, \tilde{N}_0)$, with $\tilde{N}_0 = \gamma/(2\gamma - G)$. This leads to a linear operator \mathcal{L}_V [34], which governs fluctuations on \mathcal{M} near \mathbf{V}_V . Importantly, the structure of \mathcal{L}_V is qualitatively distinct from that of $\hat{\mathcal{L}}_F$ for the ferromagnetic phase. The vortex phase is found to be destabilized when

$$G(G + 4\gamma)^2 + 72(D + J/\sqrt{3})^2(G + \gamma) < 0. \quad (9)$$

We show this instability boundary in Fig. 4(a) for different exchange coupling J . We stress that this condition differs markedly from that of the ferromagnetic state (8), which is not surprising since the analysis is carried out around different fixed points. It is clear that in certain parameter region, both vortex and ferromagnetic phases are stable, which gives rise to the hysteresis discussed below. This is in sharp contrast to the nonreciprocal Kuramoto model [34], where the transition is symmetric and the instability is always triggered at $G = 0$ from both directions as shown in the upper panel of Fig. 4(b). The different nonlinearity around different phases leads to hysteretic behavior: the onset of instability depends on the direction of the transition, shown in the lower panel of Fig. 4(b). In other words, both the ferromagnetic and (anti)vortex states can coexist as stable fixed points for the same parameters [34], and the selected state depends on the history (initial condition or sweep direction), giving rise to hysteretic phenomena.

We present the phase diagram in Fig. 4(c) for $J = 0$, obtained by solving the dynamics numerically by starting from the vortex phase in contrast to Fig. 2(a) where we start from a ferromagnetic state. The yellow curve in Fig. 4(c) shows the analytically obtained instability boundary (9), which agrees well with the numerics. We note that the vortex state persists within a finite window of negative dissipative coupling, $G < 0$. This stability, absent in the nonreciprocal Kuramoto model [34], stems from dynamical feedback: the always-stable number sector (\mathbb{R}_+^3) couples to the phase sector (\mathbb{T}^2) via the antisymmetric exchange D , effectively renormalizing the phase dynamics and shifting the vortex instability to more negative G . A larger D strengthens this feedback, further widening the stability window as observed in Fig. 4(c). This vortex phase is characterized by a rotating Goldstone mode Φ with frequency $\Omega = J + \sqrt{3}D$. As a result, time-translation symmetry is spontaneously broken, while the global U(1) symmetry is dynamically restored on average. We show the stabilization of this chiral vortex state, with an initial condition close to the vortex fixed point, in Supplemental Video 4 [34].

The emergence of the ac phase hinges on the strength of D . For small $|D|$, coupling between phase (\mathbb{T}^2)

and density (\mathbb{R}_+^3) dynamics is insufficient to stabilize a limit cycle, causing a direct collapse from the vortex into a static ferromagnetic state, where global U(1) symmetry is broken but time-translation symmetry is restored. Once $|D|$ exceeds a critical threshold, a Poincaré–Andronov–Hopf bifurcation gives rise to a stable limit cycle in the five-dimensional reduced phase space \mathcal{M} , thereby generating an ac phase that intervenes between the vortex and ferromagnetic regions.

Importantly, this regime differs from the ac phase nucleated by instability of the ferromagnetic state: here, the trajectory explores a distinct region of phase space \mathcal{M} , as revealed by projections onto the \mathbb{T}^2 submanifold [Fig. 4(e)]. This ac phase exhibits robustness against small variations in the coupling strengths [34], indicating that it does not rely on fine-tuning and should be accessible in realistic settings. This ac phase again is distinguished by the appearance of two emergent frequencies (see Supplemental Video 5 [34]), spontaneously breaking time-translation symmetry. In addition to the global U(1) Goldstone mode, a second frequency arises from stable limit cycles in the phase space \mathcal{M} . As shown in Fig. 4(d), this limit cycle frequency grows with D but exhibits nonlinear dependence on other coupling parameters. As one decreases $|D|$, the amplitude of the trajectory grows [see Fig. 4(e) inset], until a global bifurcation abruptly ejects the system into the ferromagnetic fixed point (see Supplemental Video 6 [34]), marking a sharp boundary for the ac phase.

Our results reveal that the interplay between nonreciprocity and nonlinearity can serve as a robust mechanism to engineer novel spontaneous dynamical phenomena, which may be explored in diverse experimental platforms.

Acknowledgments. We thank Even Thingstad and Kouki Nakata for insightful discussions. This work was supported by the Georg H. Endress Foundation and by the Swiss National Science Foundation, NCCR SPIN (grant number 51NF40-180604).

- [1] B. D. Josephson, Possible new effects in superconductive tunnelling, *Physics letters* **1**, 251 (1962).
- [2] J. R. Anglin and W. Ketterle, Bose–einstein condensation of atomic gases, *Nature* **416**, 211 (2002).
- [3] H. Deng, H. Haug, and Y. Yamamoto, Exciton-polariton bose-einstein condensation, *Reviews of modern physics* **82**, 1489 (2010).
- [4] J. Bloch, I. Carusotto, and M. Wouters, Non-equilibrium bose-einstein condensation in photonic systems, *Nature Reviews Physics* **4**, 470 (2022).
- [5] S. O. Demokritov, V. E. Demidov, O. Dzyapko, G. A. Melkov, A. A. Serga, B. Hillebrands, and A. N. Slavin, Bose–einstein condensation of quasi-equilibrium magnons at room temperature under pumping, *Nature* **443**, 430 (2006).

[6] D. A. Bozhko, A. A. Serga, P. Clausen, V. I. Vasyuchka, F. Heussner, G. A. Melkov, A. Pomyalov, V. S. L'vov, and B. Hillebrands, Supercurrent in a room-temperature bose-einstein magnon condensate, *Nature Physics* **12**, 1057 (2016).

[7] A. J. Kreil, H. Y. Musiienko-Shmarova, P. Frey, A. Pomyalov, V. S. L'vov, G. A. Melkov, A. A. Serga, and B. Hillebrands, Experimental observation of josephson oscillations in a room-temperature bose-einstein magnon condensate, *Physical Review B* **104**, 144414 (2021).

[8] H.-I. Lu, M. Schemmer, L. M. Aycock, D. Genkina, S. Sugawa, and I. B. Spielman, Geometrical pumping with a bose-einstein condensate, *Physical review letters* **116**, 200402 (2016).

[9] J. Keeling and N. G. Berloff, Spontaneous rotating vortex lattices in a pumped decaying condensate, *Physical review letters* **100**, 250401 (2008).

[10] M. Szymańska, J. Keeling, and P. Littlewood, Nonequilibrium quantum condensation in an incoherently pumped dissipative system, *Physical review letters* **96**, 230602 (2006).

[11] J. Zou, S. Bosco, E. Thingstad, J. Klinovaja, and D. Loss, Dissipative spin-wave diode and nonreciprocal magnonic amplifier, *Phys. Rev. Lett.* **132**, 036701 (2024).

[12] H. Yuan, R. Lavrijsen, and R. Duine, Unidirectional magnetic coupling induced by chiral interaction and nonlocal damping, *Physical Review B* **107**, 024418 (2023).

[13] A. Metelmann and A. A. Clerk, Nonreciprocal photon transmission and amplification via reservoir engineering, *Physical Review X* **5**, 021025 (2015).

[14] F. Reiter, D. Reeb, and A. S. Sørensen, Scalable dissipative preparation of many-body entanglement, *Physical review letters* **117**, 040501 (2016).

[15] J. Zou, S. Zhang, and Y. Tserkovnyak, Bell-state generation for spin qubits via dissipative coupling, *Phys. Rev. B* **106**, L180406 (2022).

[16] J. Zou, S. Bosco, and D. Loss, Spatially correlated classical and quantum noise in driven qubits, *npj Quantum Information* **10**, 46 (2024).

[17] S. Driessens, J. Zou, E. Thingstad, J. Klinovaja, and D. Loss, Robust tripartite entanglement generation via correlated noise in spin qubits, *arXiv:2506.20466* (2025).

[18] M. Fruchart, R. Hanai, P. B. Littlewood, and V. Vitelli, Non-reciprocal phase transitions, *Nature* **592**, 363 (2021).

[19] In (b), we use $G = -1/2$, $J = -1$, $D = 1$ and initial conditions $\theta_1(0) = 0$, $\theta_2(0) = \pi/2$, $\theta_3(0) = -\pi/5$; In (c), we use $G = -1$, $J = 0$, $D = 3/2$ and initial conditions $\theta_1(0) = 0$, $\theta_2(0) = 2\pi/3 + \pi/4$, $\theta_3(0) = 7\pi/6$; In (d), we use $G = 1$, $J = 0.1$, $D = 2$ and initial conditions $\theta_1(0) = 0$, $\theta_2(0) = 0.1$, $\theta_3(0) = -0.2$. In all plots in Fig. 1, we fix $\gamma = P = 3$ and $N_1(0) = 6 \times 10^{-6}$, $N_2(0) = 3 \times 10^{-6}$, $N_3(0) = 4 \times 10^{-6}$.

[20] K. Sacha and J. Zakrzewski, Time crystals: a review, *Reports on Progress in Physics* **81**, 016401 (2017).

[21] M. P. Zaletel, M. Lukin, C. Monroe, C. Nayak, F. Wilczek, and N. Y. Yao, Colloquium: Quantum and classical discrete time crystals, *Rev. Mod. Phys.* **95**, 031001 (2023).

[22] H. Watanabe and M. Oshikawa, Absence of quantum time crystals, *Phys. Rev. Lett.* **114**, 251603 (2015).

[23] V. K. Kozin and O. Kyriienko, Quantum time crystals from hamiltonians with long-range interactions, *Phys. Rev. Lett.* **123**, 210602 (2019).

[24] Here, we identify $\psi_4 \equiv \psi_1$ and $\psi_0 \equiv \psi_3$. We also set $\hbar = 1$ in the following discussion.

[25] B. Heinrich, Y. Tserkovnyak, G. Woltersdorf, A. Brataas, R. Urban, and G. E. Bauer, Dynamic exchange coupling in magnetic bilayers, *Physical Review Letters* **90**, 187601 (2003).

[26] K. Nakata, J. Zou, J. Klinovaja, and D. Loss, Magnonic φ josephson junctions and synchronized precession, *Physical Review Research* **6**, 033207 (2024).

[27] T. Yu, J. Zou, B. Zeng, J. Rao, and K. Xia, Non-hermitian topological magnonics, *Phys. Rep.* **1062**, 1 (2024).

[28] P. Yang, X. Xia, H. He, S. Li, X. Han, P. Zhang, G. Li, P. Zhang, J. Xu, Y. Yang, and T. Zhang, Realization of nonlinear optical nonreciprocity on a few-photon level based on atoms strongly coupled to an asymmetric cavity, *Phys. Rev. Lett.* **123**, 233604 (2019).

[29] B. Zhen, C. W. Hsu, Y. Igarashi, L. Lu, I. Kaminer, A. Pick, S.-L. Chua, J. D. Joannopoulos, and M. Soljačić, Spawning rings of exceptional points out of dirac cones, *Nature* **525**, 354 (2015).

[30] M.-A. Miri and A. Alu, Exceptional points in optics and photonics, *Science* **363**, eaar7709 (2019).

[31] W. Gou, T. Chen, D. Xie, T. Xiao, T.-S. Deng, B. Gadway, W. Yi, and B. Yan, Tunable nonreciprocal quantum transport through a dissipative aharonov-bohm ring in ultracold atoms, *Physical review letters* **124**, 070402 (2020).

[32] Q. Liang, D. Xie, Z. Dong, H. Li, H. Li, B. Gadway, W. Yi, and B. Yan, Dynamic signatures of non-hermitian skin effect and topology in ultracold atoms, *Phys. Rev. Lett.* **129**, 070401 (2022).

[33] M. Reisenbauer, H. Rudolph, L. Egyed, K. Hornberger, A. V. Zasedatelev, M. Abuzarli, B. A. Stickler, and U. Delić, Non-hermitian dynamics and non-reciprocity of optically coupled nanoparticles, *Nature Physics* **20**, 1629 (2024).

[34] In the supplemental material, we include detailed discussions on (i) nonreciprocal kuramoto model, (ii) instability of the ferromagnetic phase, and (iii) instability of the vortex phase. we also include all mathematica codes used to generate the figures in the main text. in supplemental videos 1-3, we show the demonstrations of the chiral ferromagnetic rotation, the ac phase with two emergent frequencies, and the chiral vortex phase emerging in the condensate dynamics, starting from initial conditions near the ferromagnetic fixed point. in supplemental videos 4-6, we show the demonstrations of the chiral vortex phase, the ac phase with two emergent frequencies, and the ferromagnetic phase, starting from initial conditions near the vortex fixed point..

[35] Here we use the initial conditions: $N_1(0) = 6 \times 10^{-6}$, $N_2(0) = 3 \times 10^{-6}$, $N_3(0) = 4 \times 10^{-6}$, $\theta_{21}(0) = -0.04$, and $\theta_{32}(0) = 0.05$.

[36] We note that the generalized Josephson equations depend only on the relative phases of the three condensates. The center-of-mass phase is a zero mode and does not affect the dynamics.

[37] S.-N. Chow and J. K. Hale, *Methods of bifurcation theory*, Vol. 251 (Springer Science & Business Media, 2012).

[38] We use initial conditions near the vortex fixed point: $\theta_{21}(0) = 2\pi/3 - 0.03$, $\theta_{32}(0) = 2\pi/3 + 0.04$, $N_1(0) = 6 \times 10^{-6}$, $N_2(0) = 3 \times 10^{-6}$, and $N_3(0) = 4 \times 10^{-6}$.